Earthquakes and Structures, *Vol. 17, No. 5 (2019) 489-499*
DOI: https://doi.org/10.12989/eas.2019.17.5.489

Ratcheting behavior of 90° elbow piping under seismic loading

Xiaohui Chen*[1,2], Kaicheng Huang[1], Sheng Ye[1], Yuchen Fan[1,3] and Zifeng Li[2]

[1]*School of Control Engineering, Northeastern University, Qinhuangdao, 066004, China*
[2]*School of Mechanical Engineering, Yanshan University, Qinhuangdao, 066004, China*
[3]*College of Energy Engineering, Zhejiang University, Zhejiang, 310058, China*

(*Received June 4, 2019, Revised September 24, 2019, Accepted September 26, 2019*)

Abstract. Elastic-plastic behavior of nuclear power plant elbow piping under seismic loads has been conducted in this study. Finite element analyses are performed using classical Bilinear kinematic hardening model (BKIN) and Multilinear kinematic hardening model (MKIN) as well as a nonlinear kinematic hardening model (Chaboche model). The influence of internal pressure and seismic loading on ratcheting strain of elbow pipe is studied by means of the three models. The results found that the predicted results of Chaboche model is maximum, closely followed by the predicted results of MKIN model, and the minimum is the predicted results of BKIN model. Moreover, comparisons of analysis results for each plasticity model against predicted results for a equivalent cyclic loading elbow component and for a simplified piping system seismic test are presented in the paper.

Keywords: pressurized pipe; seismic loading; finite element analysis; constitutive model; ratcheting strain

1. Introduction

The ratcheting is a phenomenon for the asymmetrical stress-controlled cycling and is important in designing engineering structural components. Piping systems, especially elbows are an important part of power plants components. In addition to fluid pressure, piping components have to endure bending loads due to seismic loading. When these components are cyclically loaded in the plastic regime, progressive plastic deformation can occur by a combination of primary(steady) loading and secondary (cyclic) loading. This phenomenon is called as ratcheting effect.

Many efforts have been made by some scholars to understand the ratcheting phenomena of pressurized pipes. For example, Vishnuvardhan *et al*. (2012) studied ratcheting behavior of Type 304LN stainless steel elbows subjected to steady internal pressure and opening and closing cyclic bending at ambient temperature. The results observed that maximum strain was observed at the intrados and crown locations of the elbows and minimum strain occurred at the extrados location. Crack was observed in the bent portion at one of the crown locations in all the four specimens. The ratcheting strain increased with the increasing of the number of cycles at crown and intrados locations. However, the strain accumulation rate decreased with number of cycles. The elbow specimens have failed by occurrence of through-wall axial crack accompanied by simultaneous ballooning. Vishnuvardhan *et al*. (2013) observed ratcheting strain of Type 304LN stainless steel straight pipes and elbows subjected to steady internal pressure and cyclic bending load. The results indicated that the specimens undergo significant ratchet swelling (ballooning), ovalization and consequent thinning of the cross-section during ratcheting. The straight pipes failed either by occurrence of through-wall crack accompanied by simultaneous ballooning, or bursting with simultaneous ballooning. All the elbows failed by occurrence of through-wall crack accompanied by simultaneous ballooning. Ratcheting behaviour of straight pipes and elbows were compared and it was generally inferred that ratcheting was more pronounced in straight pipes than in elbows. Chen *et al*. (2013) summarized the experimental investigation and finite element analysis (FEA) of ratcheting behavior of pressurized piping. Based on experimental and FEA research, ratcheting boundaries have been determined with the final aim of aiding the safety design and assessment of engineering piping structures. Zakavi *et al*. (2014) simulated cyclic loading behavior of carbon steel pressurized piping by means of kinematic hardening model, the piping were subjected to internal pressure and seismic bending. Karamanos (2016) reviewed the mechanical behavior of steel pipe (elbows) based on analytical solutions, numerical results and experimental data. The main feature of pipe bends under bending loading (in-plane and out-of-plane) was cross-sectional ovalization, which influenced bending capacity and was affected by internal pressure level. Bends subjected to cyclic in-plane bending exhibited fatigue damage, leading to base metal cracking at the elbow flanks. Varvani-Farahani and Nayebi (2018) reviewed ratcheting response of materials involving various influential parameters such as loading spectra, thermal cycles, stress levels, stress raisers, strain rate, and visco-plasticity and material types with a focus on pressurized pipes and equipment. Kim *et al*. (2018) measured ratcheting strain of the steel pipe elbow using the image signal. The

*Corresponding author, Ph.D.
E-mail: chenxh@neuq.edu.cn

ISSN: 2092-7614 (Print), 2092-7622 (Online)

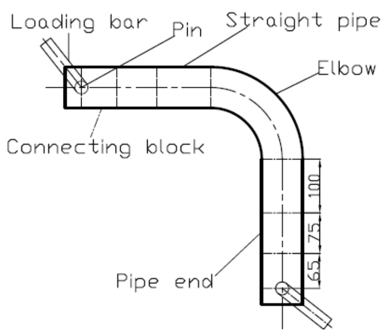

Fig. 1 Elbow specimen

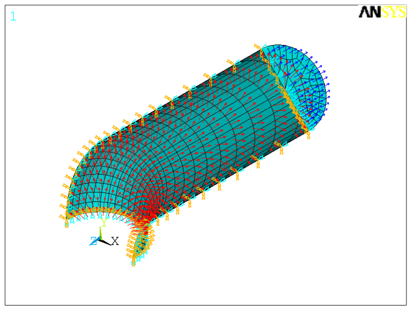

Fig. 2 Finite element model and loading

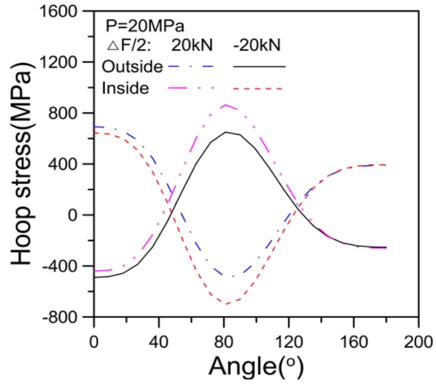

(a) Hoop stress

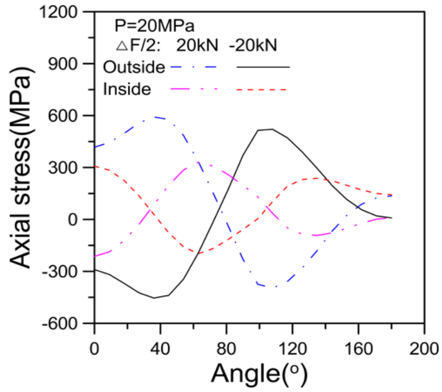

(b) Axial stress

Fig. 3 Elastic nominal stress distribution

accumulative strain was expected to be of use when estimating the failure criteria. In addition, by using the image signal, the ratcheting strain at a remote distance can be measured without the installation of a conventional sensor. Therefore, the ratcheting strain was expected to become major factor for defining the failure criteria of the piping system.

Using finite element analysis with the nonlinear isotropic/kinematic (combined) hardening model, Zakavi *et al*. (2017) studied ratcheting behavior of carbon steel (ASTM A106B) and stainless steel (304L) elbows under steady internal pressure and in-plane external moments at frequencies typical of seismic excitations. The results showed that the maximum ratcheting was occurred in the hoop direction at crown, the calculated initial ratcheting rate was large and then decreased with the increasing of cycles. However, the predicted results over estimated values comparing with the experimental data. Beden and Allawi (2017) investigated deformation behavior of thin-walled elbow under low cycle fatigue condition. The results showed that the strain occurred at the inner and outer surfaces of the elbow pipe for the locations at crown, intrados and extrados. The resulted revealed that different elbows showed the fatigue life behavior based on different locations. The simulation results showed that more studies on the piping elbows need to be perfumed in order to obtain more accurate fatigue life.

2. Finite element analysis

Stainless steel Z2CND18.12N elbow specimen is used in this study. The chemical compositions were given in the reference (Chen *et al*. 2016). The specimens were constructed of 76 mm diameter, 4.5 mm in nominal thickness, 90 degree, long radius (mean bend radius 95 mm) elbow pipe, each of which was butt welded to a 100 mm long straight pipe, as shown in Fig. 1.

2.1 Static analysis

Moreton *et al*. (1996) simulated the stress distribution of pressurized long radius elbow under in-plane bending by elastic finite element analysis. It was shown that the most likely suffering ratcheting strain could occur at flanks and midway between intrados and flanks. Fig. 3 gives the elastic stress distributions of elbow pipe subjected to inner pressure of 20 MPa and a bending loading of 20 kN. It is found that the elastic stress distribution of elbow pipe is the same as that of Moreton's. In future experiment, the strain gauges are distributed in the positions of the larger stress, namely intrados (0°), 45° position at midway between flank and intrados, both flanks (90°) and extrados (180°).

2.2 Modal analysis

In order to study the effect of seismic are on ratcheting behavior of elbow pipe, modal analysis of elbow pipe is carried out, and natural period of vibration is obtained, as listed in Table 1.

3. Transient dynamic analysis

The earthquake originates from the depths of the earth's

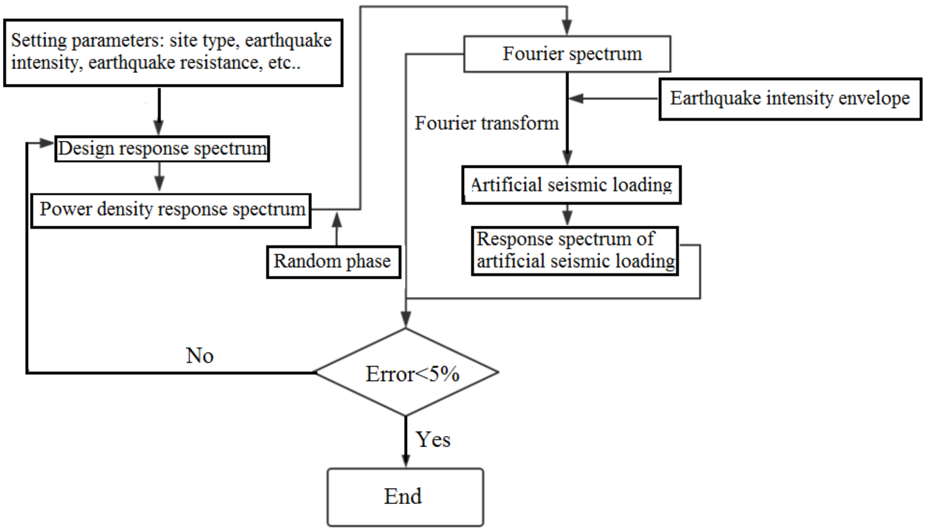

Fig. 4 A-1 Flow chart of artificial seismic loading

Table 1 Natural period of vibration

SET	FREQ	LOAD STEP	SUBSTEP	CUMULATIVE
1	0.000	1	1	1
2	0.94248E-05	1	2	2
3	0.044972	1	3	3
4	30.192	1	4	4
5	227.35	1	5	5
6	329.49	1	6	6
7	853.83	1	7	7
8	1095.3	1	8	8
9	1601.1	1	9	9
10	1749.2	1	10	10

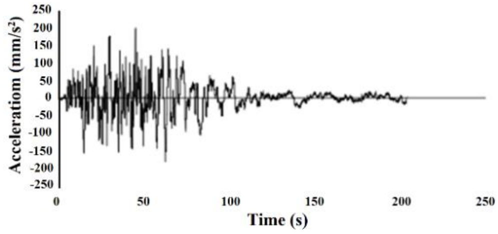

Fig. 5 A-1 seismic loading

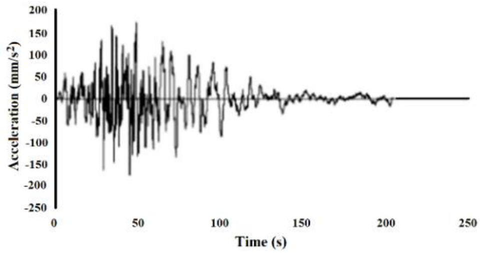

Fig. 6 A-2 seismic loading

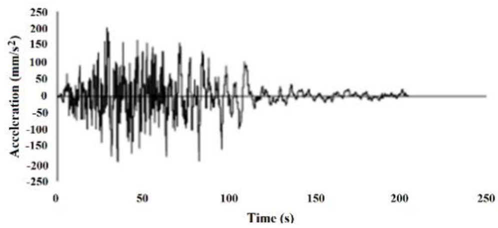

Fig. 7 A-3 seismic loading

crust. When the earthquake occurs, seismic wave is generated. By means of the rock or soil of the earth's crust, seismic wave is spread to earth's surface. When seismic wave is spread to earth's surface, sudden shaking of the ground is caused. Thus, it makes sudden shaking of the buildings or equipment on the ground.

When the earthquake occurs, seismic ground motion is a complex space motion which is divided into three translation component and three rotational components. In the view of rarely measured data of rotational component, the calculated seismic loading generally is not considered. The ground horizontal motion makes the equipment to produce horizontal vibration, its harm is bigger. The harm of vertical vibration is less than that of horizontal vibration. Therefore, horizontal vibration is studied in the paper.

In order to improve wide range of application, artificial seismic loading is constituted in this study, as given in Fig. 4.

According to the earthquake related parameters of main country/town, three different seismic loadings are constituted in this study, design earthquake group is the second group, site category for II class, as shown in Fig. 5-Fig. 7. The frequency content of the seismic waves are tuned to be close to the piping fundamental frequency, which was approximately 10 Hz. Fig. 5 is constituted based on basic acceleration level of 0.2 g and the seismic fortification intensity of 8 degrees, which is called as A-1 seismic loading with peak acceleration as +196.94/-182.26. Fig. 6 is constituted based on basic acceleration level of 0.15 g and the seismic fortification intensity of 7 degrees, which is called as A-2 seismic loading with peak acceleration as +151.35/-176.58. Fig. 7 is constituted based on basic acceleration level of 0.2 g and the seismic fortification intensity of 8 degrees, which is called as A-3 seismic loading with peak acceleration as +195.52/-192.15. In the light of the above artificial seismic loading,

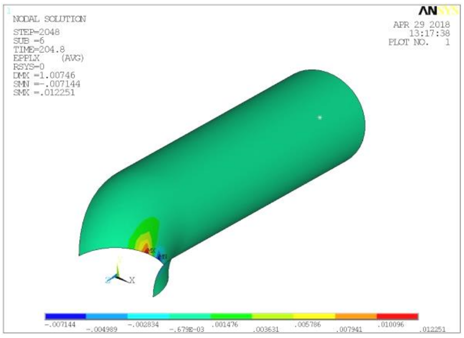

Fig. 8 Plastic strain contour under A-1 seismic loading using BKIN model

ratcheting effect of elbow pipe under internal pressure and seismic loading was simulated using BKIN model, MKIN model and Chaboche model in ANSYS software.

3.1 Bilinear kinematic hardening model (BKIN)

The stress-strain curve from a monotonic uniaxial tensile test of a Z2CND18.12N austenitic stainless steel test specimen was used to define the parameters for BKIN model (Chen *et al*. 2016). The parameters included elastic modulus E=1.95×10^5 MPa, yield stress 360 MPa, plastic modulus 2280 MPa.

3.1.1 Effect of seismic loading on ratcheting strain of elbow

The plastic strain contour of 90° elbow pipe under 1.98 MPa internal pressure and A-1 seismic loading is given in Fig. 8. It can be seen from Fig. 8 that the maximum ratcheting strains occur at flanks of 90° elbow pipe.

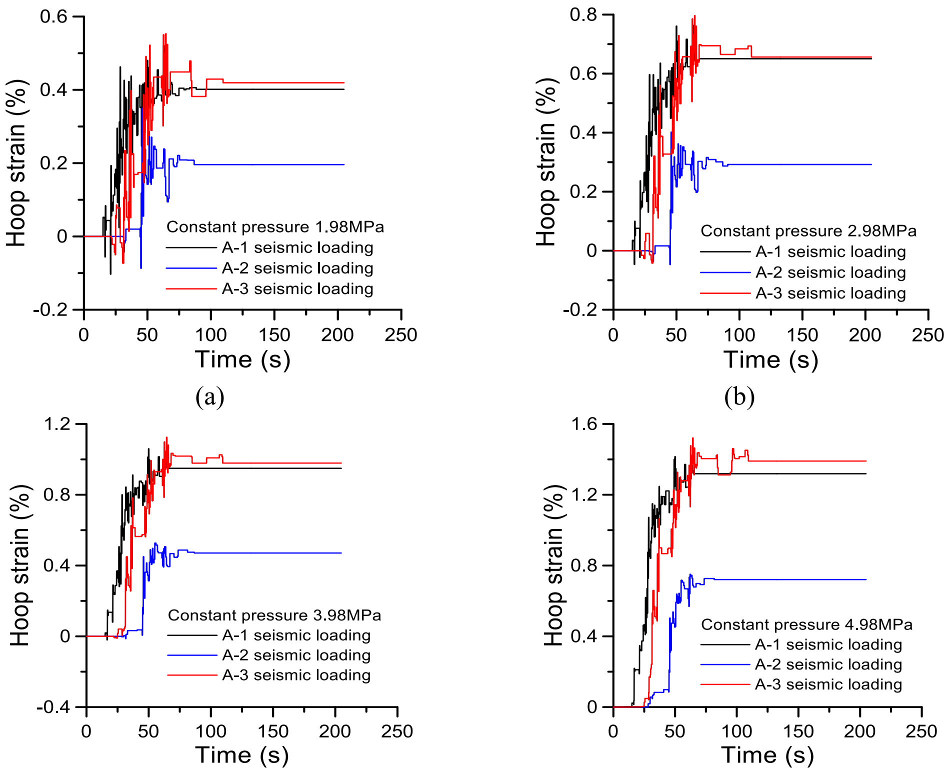

(a) (b)

(c) (d)

Fig. 9 Ratcheting strain under different seismic loading using BKIN model

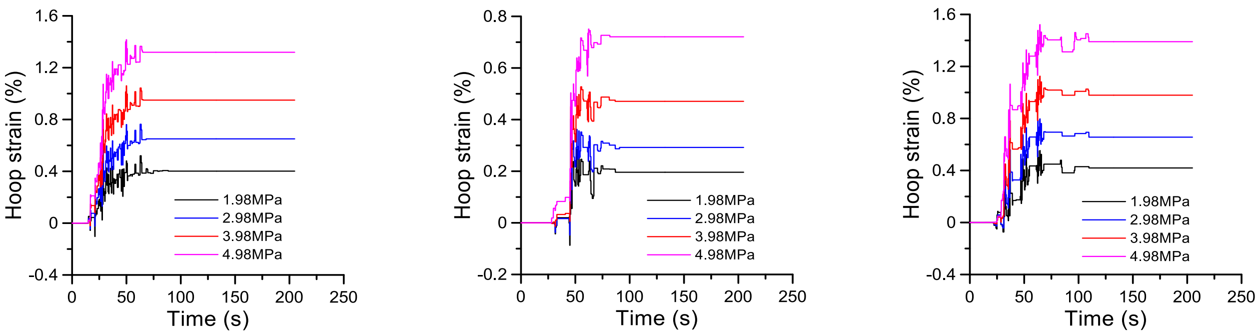

(a) A-1 seismic loading (b) A-2 seismic loading (c) A-3 seismic loading

Fig. 10 Ratcheting strain under different internal pressure using BKIN model

Table 2 MKIN stress-strain values

Strain (%)	Stress (MPa)	Strain (%)	Stress (MPa)	Strain (%)	Stress (MPa)
0.000	0	0.280	320	1.305	400
0.125	250	0.405	340	2.285	440
0.225	290	0.512	352	2.515	450

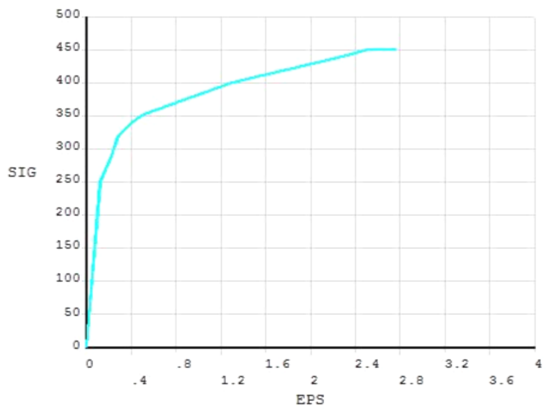

Fig. 11 Stress-strain curve of MKIN model

Ratcheting strain occurs mainly at flank of 90° elbow pipe using BKIN medel. Fig. 9 shows the effect of seismic loading on ratcheting strain of 90° elbow pipe. It indicates that ratcheting strain of 90° elbow pipe under the same internal pressure and A-3 seismic loading is larger than those of others. The ratcheting strain of 90° elbow pipe under A-2 seismic loading is the smallest.

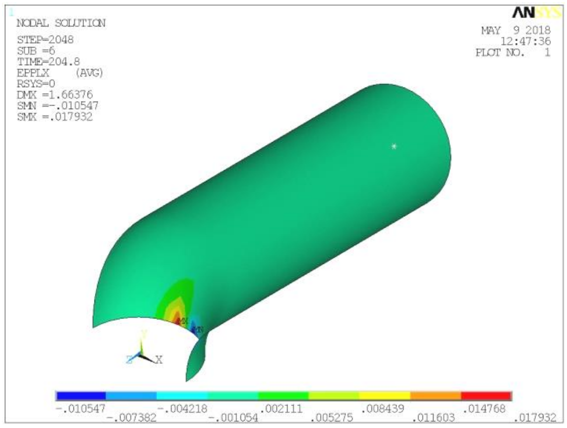

Fig. 13 Plastic strain contour under A-1 seismic loading using MKIN model

3.1.2 Effect of internal pressure on ratcheting strain of elbow

Fig. 10 shows strain-time curve of 90° elbow pipe subjected to the seismic loading A-1, A-2 and A-3 respectively and different internal pressure. It is found that f seismic loading has effect on ratcheting strain at flank of 90° elbow pipe. It indicates that ratcheting strain of 90° elbow pipe under the 4.98 MPa internal pressure is larger than those of others. The ratcheting strain of 90° elbow pipe under 1.98 MPa internal pressure is the smallest.

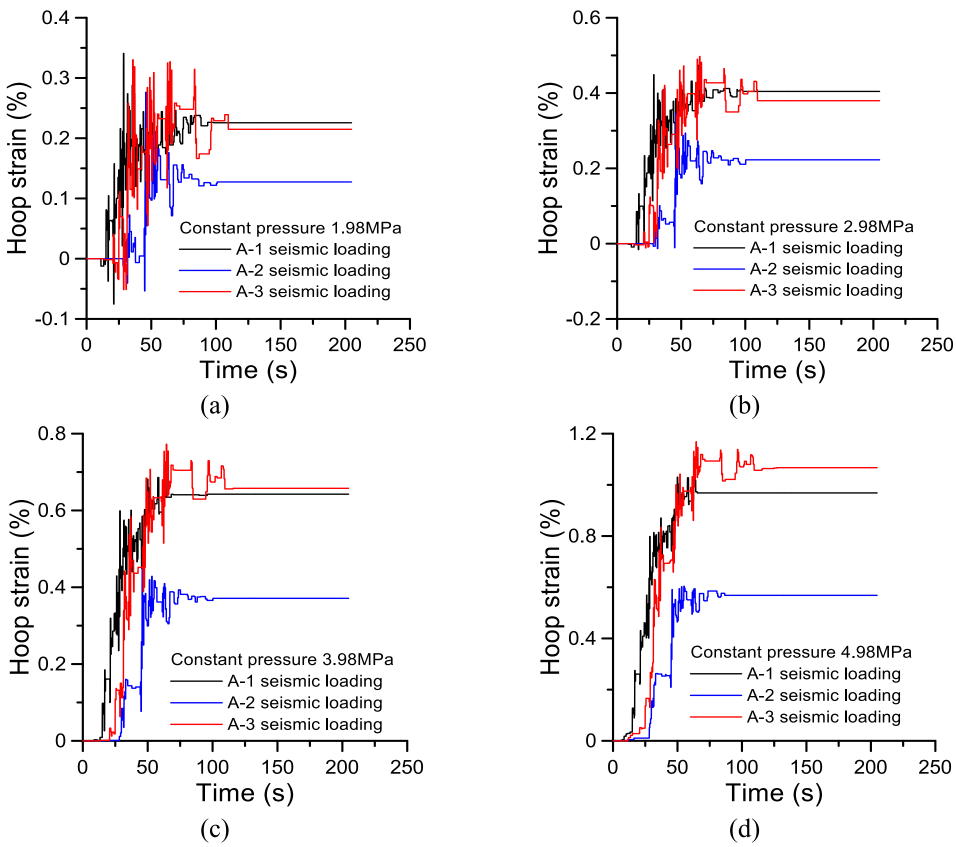

Fig. 12 Ratcheting strain under different seismic loading using MKIN model

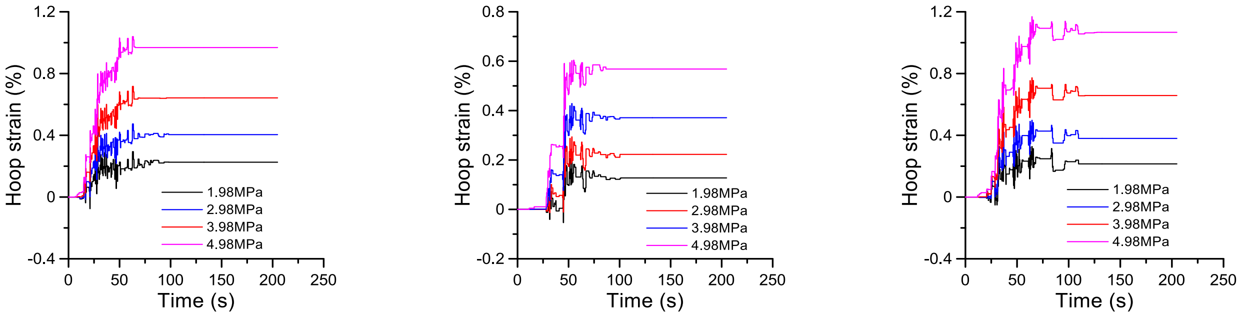

(a) A-1 seismic loading (b) A-2 seismic loading (c) A-3 seismic loading

Fig. 14 Strain-time curve under different internal pressure

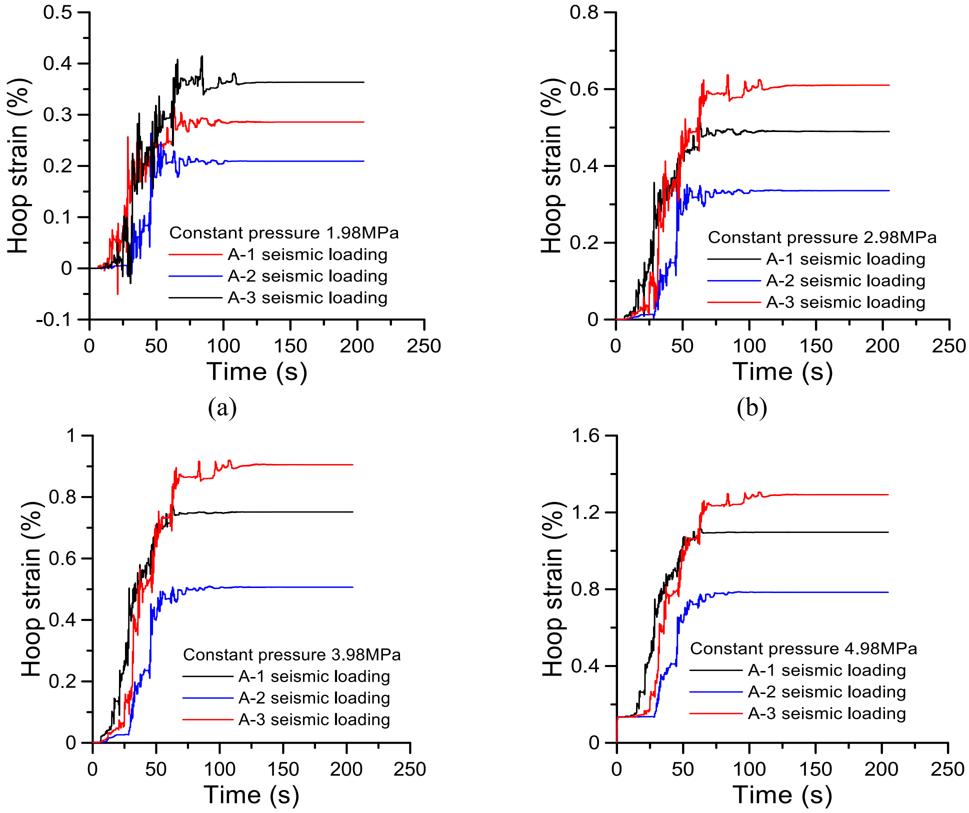

(a) (b) (c) (d)

Fig. 15 Strain-time curve under different seismic loading using CHABOCHE model

3.2 Multilinear kinematic hardening model (MKIN)

The stress-strain curve from a monotonic uniaxial tensile test of a Z2CND18.12N austenitic stainless steel test specimen is used to define the parameters for MKIN model. The stress-strain curve is approximated by nine linear segments from zero to 2.5 percent strain as shown in Fig. 11.

3.2.1 Effect of seismic loading on ratcheting strain of elbow

It can be seen from Fig. 13 that the maximum ratcheting strains occur at flanks of 90° elbow pipe. Ratcheting strain occurs mainly at flank of 90° elbow pipe. Therefore, only ratcheting strains at flanks are compared below using BKIN model.

Fig. 12 shows the influence of seismic loading on ratcheting strain of 90° elbow pipe. It indicates that ratcheting strain at flank of 90° elbow pipe under the same internal pressure and A-1 seismic loading is larger than those of others. The ratcheting strain of 90° elbow pipe under A-2 seismic loading is the smallest.

3.2.2 Effect of internal pressure on ratcheting strain of elbow

Fig. 14 shows hoop plastic strain contour and Strain-time curve of 90° elbow pipe subjected to different internal pressure and seismic loading A-1, A-2 and A-3 respectively. Fig. 14 shows more significant differences in strain ratcheting behavior between the different seismic loading results. Under the same seismic loading, hoop plastic strain increases with the increasing of internal pressure.

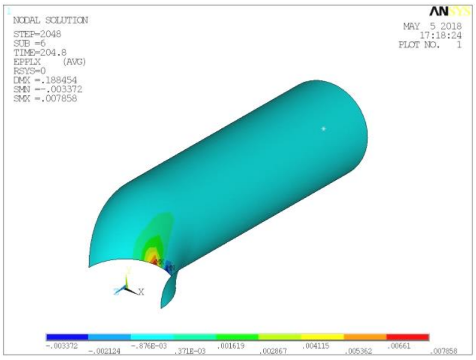

Fig. 16 Plastic strain contour under 1.98 MPa using CHABOCHE model

3.3 CHABOCHE nonlinear hardening model

The CHABOCHE model requires the definition of elastic modulus, yield stress, and the parameters C_i and γ_i for each of the three Armstrong-Frederick hardening rule. A procedure for determination of the parameters C_i and γ_i was described by Bari and Hassan (2000). The parameters of the CHABOCHE model are as follows: σ_0=270 MPa, E=2.03×10^5 MPa, C_1=70000 MPa, C_2=30000 MPa, C_3=1200 MPa, γ_1=3500, γ_2=210, γ_3=1.

3.3.1 Effect of seismic loading on ratcheting strain of elbow

The effect of internal pressure on ratcheting strain of 90° elbow pipe is given in Fig. 15. Fig. 15 shows hoop plastic strain contour and strain-time curve of 90° elbow pipe subjected to the same internal pressure and different seismic loading. A comparison of the strain results shown in Fig. 15 shows more significant differences in strain ratcheting behavior between the different analysis model results. Under the same internal pressure, hoop plastic strain changes with the changing of seismic loading.

3.3.2 Effect of internal pressure on ratcheting strain of elbow

The effect of internal pressure on ratcheting strain of 90° elbow pipe is given in Fig. 16. Fig. 16 shows hoop plastic strain contour, and Fig. 17 gives hoop strain-time curve of 90° elbow pipe subjected to different internal pressure and seismic loading A-1, A-2 and A-3 respectively. The test and analysis results for the high level seismic test A-1 are presented in Fig. 16 and Fig. 17 as time history plots of large mass displacement and Elbow flank hoop strain. Under the same seismic loading, hoop plastic strain increases with the increasing of internal pressure.

3.4 Comparison

Fig. 18 shows hoop plastic strain contour of 90° elbow pipe subjected to 1.98 MPa, 2.98 MPa, 3.98 MPa and 4.98 MPa internal pressure and A-1, A-2 and A-3 seismic loading. Following the analytical approach described above, a seismic analysis is performed using each of the three plastic hardening models, such as BKIN model, MKIN model and CHABOCHE model.

A comparison of the strain results is shown in Fig. 18. It indicates more significant differences in ratcheting strain between the different analysis model results. Ratcheting behavior of pressurized elbow pipe under seismic loading is simulated by BKIN model, MKIN model and CHABOCHE model. Comparison of the predicted results of BKIN model, MKIN model and CHABOCHE model, it is seen from Fig. 18 when 90° elbow pipe is subjected to A-1 seismic loading and A-3 seismic loading, the predicted results of BKIN model is maximum, closely followed by the predicted results of CHABOCHE model, and the minimum is the predicted results of MKIN model; when 90° elbow pipe is subjected to A-2 seismic loading and different internal pressure, the predicted results of CHABOCHE model is maximum, closely followed by the predicted results of BKIN model, and the minimum is the predicted results of MKIN model.

4. Ratcheting strain of pipeline under static loading

A Servo fatigue testing machine of 100 kN capacity is available in the research group for conducting experimental studies. Therefore, the authors think that seismic loading is translated into equivalent cyclic loading, and then ratcheting behavior of pipeline under equivalent cyclic loading is simulated by finite element method.

4.1 Seismic acceleration equivalent to static loading

On the basis of vibration theory, seismic force was

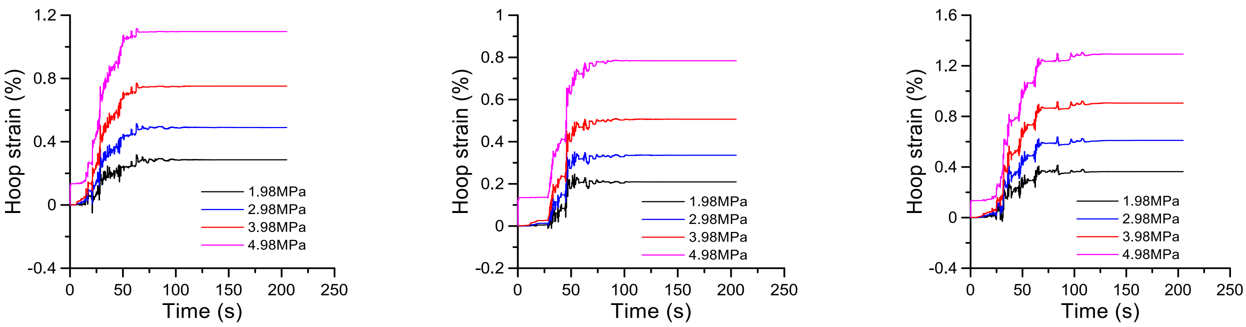

(a) A-1 seismic loading (b) A-2 seismic loading (c) A-3 seismic loading

Fig. 17 Strain-time curve under different internal pressure using CHABOCHE model

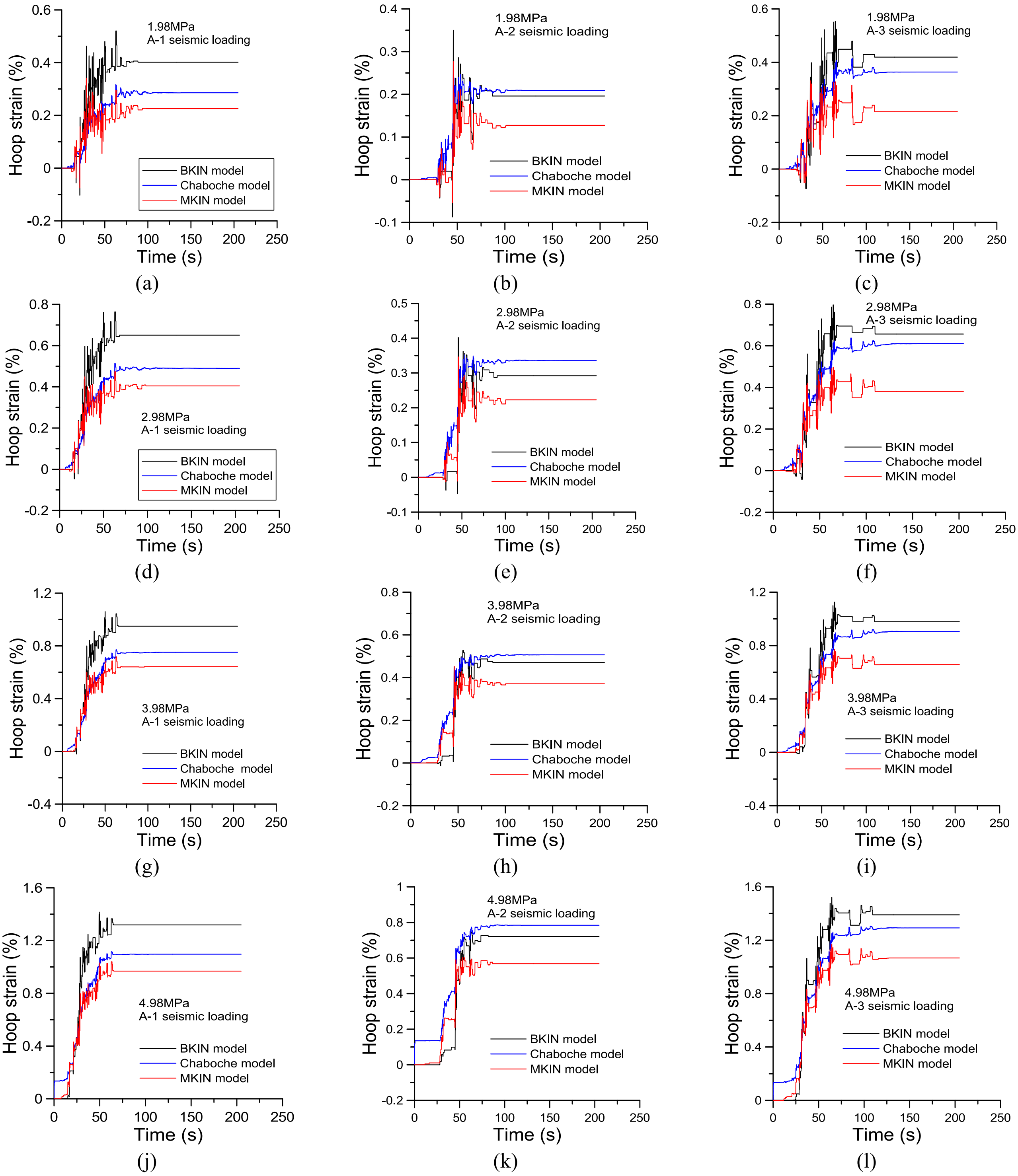

Fig. 18 Strain-time curve under different internal pressure and different seismic loading

inertial force of pipeline quality relative to the ground motion. Namely

$$F = C\alpha\eta mg \tag{1}$$

where, the parameter m represented the pipeline quality, the parameter F is that horizontal seismic force of basic mode of vibration was caused by the pipeline quality m, C represented seismic effect coefficient, usually it was 0.5. α is corresponding natural period of vibration to seismic effect coefficient, as given in Fig. 19, where the parameters $a_{\max}$ and T_g is listed in Table 3 and Table 4. The parameter η is basic modal participation factor.

According to A-2 seismic wave and Eq. (1), the pipe is laid on the site III, seismic grade is I, Seismic fortification intensity is 7 degree. On the basis of seismic response spectrum, seismic influence coefficient curve and Seismic Design Specification for Buildings, the maximum of seismic effect coefficient $a_{\max}$ is 0.08m/s^2. Where T_g=0.4 s.

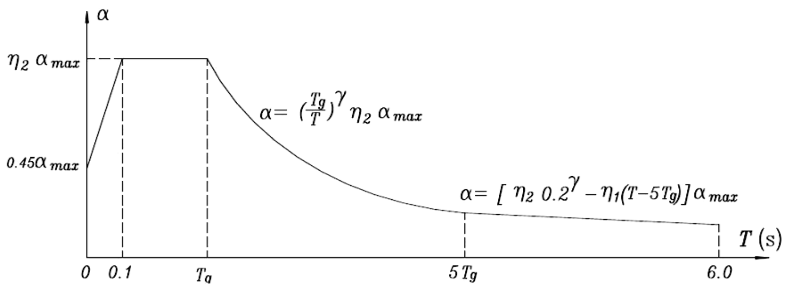

Fig. 19 Seismic influence coefficient curve

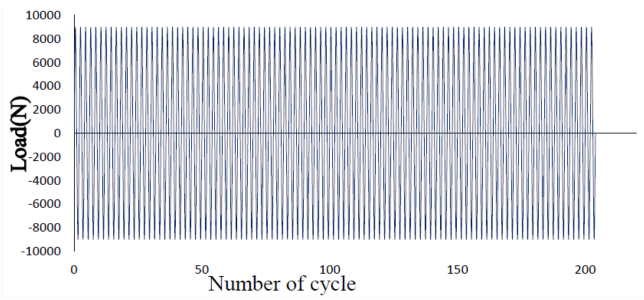

Fig. 20 Equivalent static loading

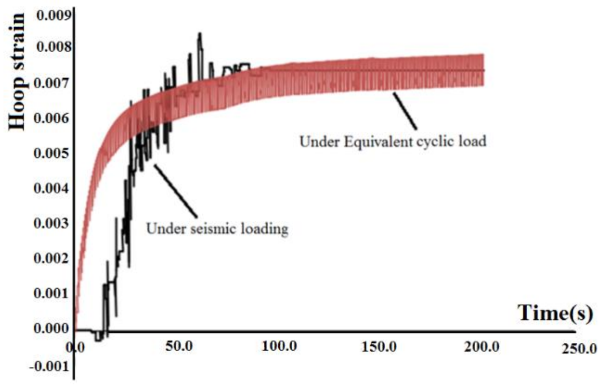

Fig. 21 Hoop plastic strain contour using BKIN model

Table 3 Maximum of seismic effect coefficient a_{max}

Site	I (Hard site)	II (Medium hard site)	III (Medium soft site)	IV (Soft site)
Near-earthquake	0.2	0.35	0.4	0.65
Near-earthquake	0.25	0.40	0.55	0.75

Table 4 Characteristic period T_g (s)

Earthquake effect	6 degree	7 degree	8 degree	9 degree
Frequent earthquake	0.04	0.08(0.12)	0.16(0.2)	0.32
Resistance earthquake	0.12	0.23(0.34)	0.45(0.68)	0.90
Rare earthquake	0.28	0.50(0.72)	0.90(1.20)	1.40

Table 5 Natural frequency, natural period and seismic effect coefficient

Set	Frequency	Period	Seismic effect coefficient
1	0.000	0.000000000000000	-203.693640000000000
2	0.94248E-05	106103.047279518000000	-1039.166610000000000
3	0.044972	22.236057991639200	883.910168000000000
4	30.192	0.033121356650768	0.053178415480000
5	227.35	0.004398504508467	0.006375995889000
6	329.49	0.003034993474764	0.000318435005300
7	853.83	0.001171193328883	-0.000143562192200
8	1095.3	0.000912991874372	-0.000245385023900
9	1601.1	0.000624570607707	-0.000298759719500
10	1749.2	0.000571689915390	0.000260045895800

Seismic influence coefficient is expressed as follows.

$$a = \begin{cases} 0.036 + 0.44T(0 \le T < 0.1) \\ 0.08(0.1 \le T < 0.4) \\ 0.08 \times \left(\frac{0.4}{T}\right)^{0.9} (0.4 \le T < 3) \end{cases} \tag{2}$$

According to the results of model analysis, Table 5 listes natural frequency, natural period and seismic effect coefficient.

Seismic effect coefficient represents the ratio of vibration energy of some vibration type in vibration system and total vibration energy. The bigger the ratio is, the bigger the influence of the corresponding type is. Therefore, based on the seismic effect coefficient and period of third vibration type, namely η=883.92 and T=22.3 s, combining with Eq. (2), seismic effect coefficient is α=0.016. Thus equivalent static loading is 9 KN. In the following, ratcheting behavior of pipeline under equivalent cyclic loading is simulated by finite element method. Seismic loading is replaced by equivalent cyclic loading which is applied in sinusoidal wave. Its period is 2s, the number of cycles is 200.

4.2 Result analysis

4.2.1 Predicted results of BKIN model

By means of BKIN model in ANSYS software, Fig. 21 compares ratcheting behavior at flank of pressurized elbow pipe subjected to equivalent cyclic loading with that under seismic loading. The results indicate that evolution law of ratcheting behavior of pressurized elbow pipe matched well.

4.2.2 Predicted results of MKIN model

On the basis of MKIN model in ANSYS software, Fig. 22 compares ratcheting behavior at flank of pressurized elbow pipe subjected to equivalent cyclic loading with that under seismic loading. The results indicate that evolution law of ratcheting behavior of pressurized elbow pipe matched well.

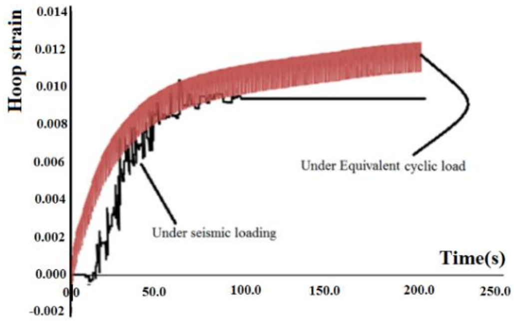

Fig. 22 Hoop plastic strain contour using MKIN model

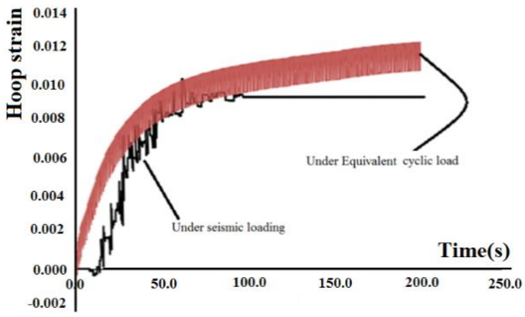

Fig. 23 Hoop plastic strain contour using CHABOCHE model

4.2.3 Predicted results of CHABOCHE model

In the light of CHABOCHE model in ANSYS software, Fig. 23 compares ratcheting behavior at flank of pressurized elbow pipe subjected to equivalent cyclic loading with that under seismic loading. The results indicate that evolution law of ratcheting behavior of pressurized elbow pipe matched well.

4.3 Comparison

Ratcheting behavior of pressurized elbow pipe under equivalent cyclic loading is simulated by BKIN model, MKIN model and CHABOCHE model. Comparison of the predicted results of BKIN model, MKIN model and CHABOCHE model, it is seen from Fig. 24 that the predicted results of CHABOCHE model is maximum, closely followed by the predicted results of MKIN model, and the minimum is the predicted results of BKIN model.

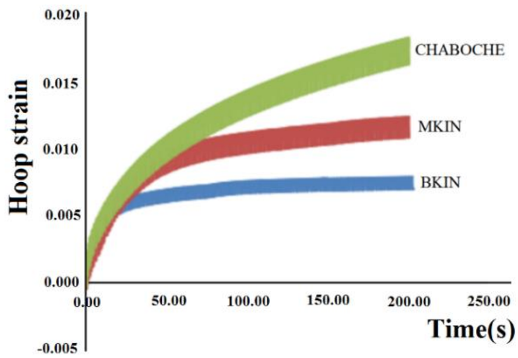

(a)

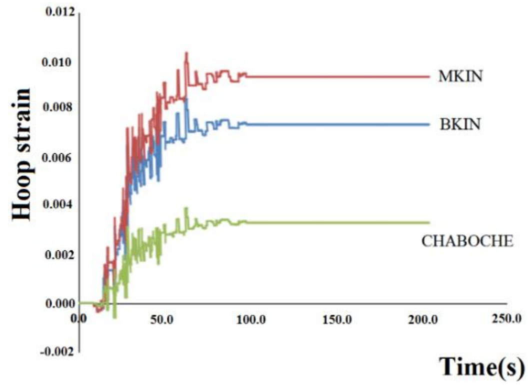

(b)

Fig. 24 Comparison of the predicted results of three models

5. Conclusions

In order to study ratcheting behavior of elbow pipe subjected to internal pressure and seismic loading, stress distributions of elbow pipe under static loading was firstly studied, and then natural period of vibration was obtained by model analysis. Furtherly, three artificial seismic loading such as A-1, A-2 and A-3 was constructed, and ratcheting behavior of elbow pipe subjected to internal pressure and three artificial seismic loading was simulated respectively with BKIN model, MKIN model and Chaboche model. The results showed when 90° elbow pipe is subjected to A-1 seismic loading and A-3 seismic loading, the predicted results of BKIN model is maximum, closely followed by the predicted results of CHABOCHE model, and the minimum is the predicted results of MKIN model; when 90° elbow pipe is subjected to A-2 seismic loading and different internal pressure, the predicted results of CHABOCHE model is maximum, closely followed by the predicted results of BKIN model, and the minimum is the predicted results of MKIN model. Moreover, the influence of internal pressure and seismic loading on ratcheting behavior of elbow pipe was investigated using BKIN model, MKIN model and Chaboche model, respectively. The results indicated that ratcheting stain for single step loading increased respectively with the increasing of seismic loading or internal pressure at the same internal pressure or seismic loading.

Finally, seismic loading is translated into equivalent cyclic loading. And then, ratcheting behavior of elbow pipe subjected to internal pressure and equivalent cyclic loading was predicted using BKIN model, MKIN model and Chaboche model. Furtherly, ratcheting behavior of pressurized elbow pipe subjected to seismic loading and equivalent cyclic loading was compared. It indicated that ratcheting behavior of pressurized elbow pipe subjected to seismic loading was in agreement well with that of equivalent cyclic loading.

Acknowledgments

This work was partly supported by the Natural Science Foundation of Hebei Province of China (No.

E2018501022), China Postdoctoral Science Foundation Funded Project (No. 2017M610171), Fundamental Research Funds for the Central Universities (No. N182304009), and 2018 Qinhuangdao College Students Science and Technology Innovation and Entrepreneurship Project (PZB1810008T-36).

References

Bari, S. and Hassan, T. (2000), "Anatomy of coupled constitutive models for ratcheting simulation", *Int. J. Plastic.*, **16**, 381-409. https://doi.org/10.1016/S0749-6419(99)00059-5.

Beden, S.M. and Allawi, M.K. (2017), "Fatigue life assessment of petroleum pipe elbows", *Int. J. Curr. Eng. Technol.*, **7**(1), 92-98.

Chen, X.H., Chen, X., Chen, G. and Li, D.M. (2016), "Evaluation of AF type cyclic plasticity models in ratcheting simulation of pressurized elbow pipes under reversed bending", *Steel Compo. Struct.*, **21**(4), 703-753. http://dx.doi.org/10.12989/scs.2016.21.4.703.

Chen, X.H., Chen, X., Yu, D.J. and Gao, B.J. (2013), "Recent progresses in experimental investigation and finite element analysis of ratcheting in pressurized piping", *Int. J. Pres. Ves. Pip.*, **101**,113-142. https://doi.org/10.1016/j.ijpvp.2012.10.008.

Karamanos, S.A. (2016), "Mechanical behavior of steel pipe bends; An overview", *J. Press. Vess.-T.*, ASME, **138**(4), 041203. https://doi.org/10.1115/1.4031940.

Kim S.W., Jeon, B.G., Chang, S.J. and Yuna, D.W. (2018), "Ratcheting strain measurement of a steel pipe elbow under in-plane cyclic loading", *Transactions of the Korean Nuclear Society Spring Meeting Jeju*, Korea, May.

Liu, C.M., Yu, D.J., Akram, W. and Chen, X. (2018), "Thermal aging effect on the ratcheting behavior of pressurized elbow pipe", *J. Press. Ves. Technol.*, **40**(2), 021604-1-9. https://doi.org/10.1115/1.4039073.

Varvani-Farahani, A. and Nayebi, A. (2018) "Ratcheting in pressurized pipes and equipment: A review on affecting parameters, modelling, safety codes, and challenges", *Fatig. Fract. Eng. Mater. Struct.*, **41**(3), 503-538. https://doi.org/10.1111/ffe.12775.

Vishnuvardhan, S., Raghava, G., Gandhi, P., Saravanan, M., Goyal, S., Arora, P., ... & Bhasin, V. (2013), "Ratcheting failure of pressurised straight pipes and elbows under reversed bending", *Int. J. Pres. Ves. Pip.*, **105-106**, 79-89. https://doi.org/10.1016/j.ijpvp.2013.03.005.

Vishnuvardhan, S., Raghava, G., Gandhi, P., Saravanan, M., Pukazhendhi, D.M., Sumit Goyal, Suneel K. Gupta, Vivek Bhasin and Vaze, K.K. (2012), "Ratcheting studies on Type 304LN stainless steel elbows subjected to combined internal pressure and in-plane bending", *J. Press. Vess.-T.*, ASME, **134**, 041203/1-10. https://doi.org/10.1115/1.4005886.

Zakavi, S.J. and Nourbakhsh, M. (2014), "The ratcheting behaviour of stainless steel pressurized piping elbows subjected to dynamic out-of-plane moments", *Modern Mech. Eng.*, **4**, 125-132. http://dx.doi.org/10.4236/mme.2014.43012.

Zakavi, S.J. and Rahmani, V. (2014), "The ratcheting rate of stainless steel pressurized piping branch under seismic loading", *Ind. J. Sci. Resea.*, **3**(1), 191-199.

Zakavi, S.J., Ajri, M. and Golshan, V. (2014), "The ratcheting behaviour of plain carbon steel pressurized piping elbows subjected to simulated seismic in-plane bending", *World J. Mech.*, **4**, 238-46. http://dx.doi.org/10.4236/mme.2014.43012.

Zakavi, S.J., Shiralivand, B. and Nourbakhsh, M. (2017), "Evaluation of combined hardening model in ratcheting behavior of pressurized piping elbows subjected to in-plane moments", *J. Comput. Appl. Res. Mech. Eng.*, **7**(1), 57-71. http://dx.doi.org/10.22061/JCARME.2017.640.

Zheng, X.T., Peng, C.F., Yu, J.Y., Wang, W., Lin, W. and Xu, J.M. (2017), "Analytical ratchet limit for pressurized pipeline under cyclic nonproportional loadings ", *J. Pip. Syst. Eng. Pract.*, **8**(3), 04017002. https://doi.org/10.1061/(ASCE)PS.1949-1204.0000260.

CC